Two- and three-body interatomic dispersion energy contributions to binding in molecules and solids

O. Anatole von Lilienfeld' and Alexandre Tkatchenko'

Articles you may be interested in

A consistent and accurate ab initio parametrization of density functional dispersion correction (DFT-D) for the 94 elements H-Pu
The Journal of Chemical Physics **132**, 154104154104 (2010); 10.1063/1.3382344

 Perspective: How good is DFT for water?
The Journal of Chemical Physics **144**, 130901130901 (2016); 10.1063/1.4944633

Two- and three-body interatomic dispersion energy contributions to binding in molecules and solids

O. Anatole von Lilienfeld[1,a)] and Alexandre Tkatchenko[2,b)]

[1]*Department of Multiscale Dynamic Materials Modeling, Sandia National Laboratories, Albuquerque, New Mexico 87185-1322, USA*
[2]*Fritz-Haber-Institut der Max-Planck-Gesellschaft, Faradayweg 4-6, D-14195 Berlin, Germany*

We present numerical estimates of the leading two- and three-body dispersion energy terms in van der Waals interactions for a broad variety of molecules and solids. The calculations are based on London and Axilrod–Teller–Muto expressions where the required interatomic dispersion energy coefficients, C_6 and C_9, are computed "on the fly" from the electron density. Inter- and intramolecular energy contributions are obtained using the Tang–Toennies (TT) damping function for short interatomic distances. The TT range parameters are equally extracted on the fly from the electron density using their linear relationship to van der Waals radii. This relationship is empirically determined for all the combinations of He–Xe rare gas dimers, as well as for the He and Ar trimers. The investigated systems include the S22 database of noncovalent interactions, Ar, benzene and ice crystals, bilayer graphene, C_{60} dimer, a peptide (Ala_{10}), an intercalated drug-DNA model [ellipticine-$d(CG)_2$], 42 DNA base pairs, a protein (DHFR, 2616 atoms), double stranded DNA (1905 atoms), and 12 molecular crystal polymorphs from crystal structure prediction blind test studies. The two- and three-body interatomic dispersion energies are found to contribute significantly to binding and cohesive energies, for bilayer graphene the latter reaches 50% of experimentally derived binding energy. These results suggest that interatomic three-body dispersion potentials should be accounted for in atomistic simulations when modeling bulky molecules or condensed phase systems. © *2010 American Institute of Physics*. [doi:10.1063/1.3432765]

I. INTRODUCTION

Noncovalent forces play an exceedingly important role for stability and functionality of many molecular as well as soft and solid condensed phase systems.[1–5] The current level of understanding of these interactions permits quantitative predictions for simple systems such as rare gases[6–8] or small molecules.[9–11] With the growing availability of ever more powerful computer hardware and computational methods, such as linear scaling electronic structure codes, increasingly realistic systems can be tackled, which are also relevant for materials science and biomolecular communities.[12–19]

Due to their electronic many-body quantum nature (dependence on excited electronic states), interatomic and intermolecular dispersion van der Waals (vdW) forces are inherently challenging to predict accurately from first principles. Although not necessarily being negligible[20] interatomic many-body contributions to dispersion forces are rarely explicitly accounted for by conventionally constructed empirical force fields designed for extended sampling of phase space. Recently, it was shown[21,22] that these forces are also largely overestimated at equilibrium distances within popular approximations of the Kohn–Sham density functional theory (KS-DFT),[23,24] frequently used for *ab initio* molecular dynamics. Even on average quite reliable quantum-chemical methods, such as second-order Møller–Plesset perturbation

theory (MP2), do not yield satisfying results for the many-body dispersion energy. Since triple and higher-order electronic excitations are explicitly required to model many-body dispersion terms, MP2 theory fails to capture the ubiquitous Axilrod–Teller–Muto triple dipole as well as higher-order terms.[25,26] Only coupled-cluster theory including single, double, and perturbative triple excitations, CCSD(T), has been shown to consistently yield accurate interactions between organic molecules.[9] Unfortunately, CCSD(T) is prohibitively expensive from the computational point of view even for moderately small systems (50–100 light atoms), not to mention the condensed phase.

For systems dominated by dispersion forces, such as rare-gas crystals, estimates of interatomic many-body contributions to cohesive energies range from 6% to 10%.[27] Ever since the seminal work of Axilrod and Teller and Muto[25,26] in 1943, attempts were made to quantify three-body contributions to rare gas systems. In this context, we only refer to studies on short and large distances[28,29] using the Kim–Gordon model,[30] on nonlocal DFT via fluctuations,[31] or on exchange contributions.[32]

In the present study, we report numerical estimates of the leading two- and three-body contributions in molecular and condensed phase systems, markedly more complex than rare gas crystals. We highlight that in contrast with other studies of *intermolecular* three-body terms such as in Ref. 33, the focus of this paper lies on *interatomic* three-body terms, in strict analogy to London's atom pairwise C_6 term.[34,35] Spe-

a)Electronic mail: oavonli@sandia.gov.
b)Electronic mail: tkatchen@fhi-berlin.mpg.de.

cifically, we will first briefly review dispersion contributions to interatomic potentials at typical equilibrium geometries using the three-body Axilrod–Teller–Muto expression.[25,26] Then, we will discuss the necessary triple dipole C_9 coefficients that are obtained in analogy to the recently devised scheme for predicting dynamic double dipole C_6 from electron densities.[36] Within this scheme, atomic C_6 and C_9 coefficients depend on the chemical environment of each atom, and therefore become functionals of the electron density. Thereafter we will shift focus to the treatment of interatomic equilibrium distances, as they occur in a broad variety of vdW systems. The two- and three-body dispersion energies are damped at short distances according to an adapted two-body potential following the work of Tang and Toennies.[6,37] For He–Xe rare gas dimer results from literature, we found a linear correlation between van der Waals radii and Tang-Toennies (TT) range parameters which we exploit to compute the range parameters from dynamic van der Waals radii (determined "on the fly" from the electron density). An interpolation of literature values for He and Ar trimers yields a similar relationship for TT range parameters that damp the three-body contribution. The first resulting dispersion energy estimates are consistent with results from symmetry-adapted perturbation theory (SAPT) where available.[38,39] We will proceed with a comparison of the two- and three-body dispersion energies to experimental or high-level theoretical binding and cohesive energies for a broad variety of systems. Numerical estimates are presented for the S22 data set,[9] a range of large molecular and condensed matter systems including bilayer graphene, ice, C_{60}-dimer, benzene crystal, dihydrofolate reductasee (DHFR) protein, double stranded DNA, α helical polyalanine decamer, intercalator drug ellipticine-DNA complex, 42 base pairs from the JSCH-2005 database,[9] and several molecular crystals from a crystal structure blind test.[40] Finally, we will discuss impact and potential future applications of the here presented scheme.

Various assumptions underlie our predictions. First of all, we use dispersion coefficients that are derived from an isotropic model of atoms in molecules (Hirshfeld partitioning). Second, all our C_6 and C_9 interactions, inter- as well as intramolecular, are assumed to be free of dynamic screening effects due to the surrounding electronic and nuclear environment. In particular, we expect this assumption to be questionable for solids where the screening is known to play a significant role.[41] Further assumptions include the specific form of the damping function, which is strictly valid only for interactions between spherical atoms. Approximations made within the determination of the dispersion coefficients according to Ref. 36 are quantified by comparison to reliable reference data for molecules.

Our main finding is that the three-body dispersion energy is not negligible even though it is generally smaller than 15% of binding or cohesive energies. For some relevant systems, however, such as bilayer graphene, this contribution can reach up to 50% of relevant binding energies. The magnitude of three-body dispersion energy can be large enough to affect rankings of energetically competing dimer conformers or molecular crystal morphologies. The two-body contribution is found in many cases to be equal or larger than the
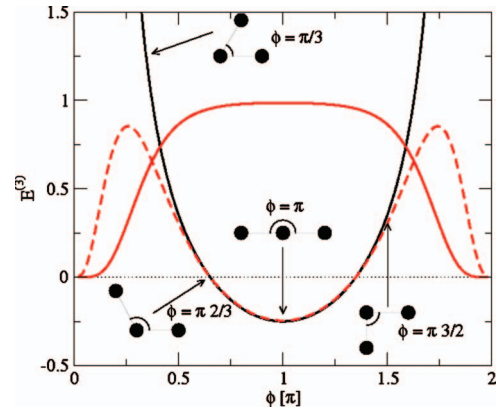

FIG. 1. Axilrod–Teller–Muto three-body energy ($E^{(3)}/C_{9_{IJK}}$) (solid black line) in an isosceles triangle as a function of ϕ according to Eq. (3) for $R_{IJ}=R_{JK}=1$. The red solid curve is the damping function of Eq. (13). The red dashed curve corresponds to the product of the two functions.

intermolecular binding energies or cohesive energies of solids, a finding that underscores the need for accurate approaches.

II. THEORY

A. Interatomic dispersion energies

The dispersion contribution to the energy of an ensemble of atoms $\{I\}$ residing at $\{\mathbf{R}_I\}$ can be written as a many-body expansion of potentials,

$$E_{\text{disp}}(\{\mathbf{R}_I\}) = \frac{1}{2}\sum_{IJ} E^{(2)}(R_I,R_J) + \frac{1}{6}\sum_{IJK} E^{(3)}(R_I,R_J,R_K) + \text{HOT},$$
(1)

where HOT are the higher order terms. In the dissociative limit or for (spherical) neutral atoms with nonoverlapping electron density these terms correspond to

$$E^{(2)}(\mathbf{R_I},\mathbf{R_J}) = -\frac{C_{6_{IJ}}}{R_{IJ}^6} - \frac{C_{8_{IJ}}}{R_{IJ}^8} - \frac{C_{10_{IJ}}}{R_{IJ}^{10}} - \text{HOT},$$
(2)

$$E^{(3)}(\mathbf{R_I},\mathbf{R_J},\mathbf{R_K}) = C_{9_{IJK}}\frac{3\cos[\phi_I]\cos[\phi_J]\cos[\phi_K]+1}{R_{IJ}^3 R_{IK}^3 R_{JK}^3} + \text{HOT},$$
(3)

where $R_{IJ}=|\mathbf{R}_I-\mathbf{R}_J|$ and $\{\phi_i\}$ are the angles in atomic triangle. The first term of the three-body dispersion contribution to the total energy of three atoms, I,J,K, is given by the Axilrod–Teller–Muto expression.[25,26] Figure 1 illustrates the behavior of this term for an isosceles triangle as a function of one angle.

B. Dispersion coefficients

The Casimir–Polder integral,

$$C_{6_{IJ}} = \frac{3}{\pi}\int_0^\infty d\omega\,\alpha_I(i\omega)\alpha_J(i\omega),$$
(4)

$$C_{9_{IJK}} = \frac{3}{\pi} \int_0^\infty d\omega \, \alpha_I(i\omega) \alpha_J(i\omega) \alpha_K(i\omega), \tag{5}$$

yields the double-dipole C_6 and triple-dipole C_9 coefficients.[25,42] $\alpha_I(i\omega)$ is the frequency-dependent dipole polarizability of site I. The difficulty consists of obtaining distributed or fragmented polarizabilities of sites in molecules.[1] For this study, we determined the $C_{9_{IJK}}$ coefficients in Eq. (3) for atoms in molecules through extension of the recently devised scheme to predict (electron-density dependent) $C_{6_{IJ}}$ coefficients.[36] We use a single-term Padé approximant[43] for $\alpha_I(i\omega)$ and the following combination rule to derive the heteronuclear $C_{9_{IJK}}$ coefficient from homonuclear $C_{9_{III}}$ values,

$$C_{9_{IJK}} = \frac{8}{3} \frac{P_I P_J P_K (P_I + P_J + P_K)}{(P_I + P_J)(P_J + P_K)(P_K + P_I)}, \tag{6}$$

with

$$P_I = C_{9_{III}} \frac{\alpha_{0,J} \alpha_{0,K}}{\alpha_{0,I}^2}, \tag{7}$$

where $\alpha_{0,I} = \alpha_I(\omega = 0)$ is the static polarizability of atom I in a molecule. See also Ref. 44 for a more complete derivation of the above combination formula.

In analogy to the previous work on C_6 coefficients,[36] we approximate the dynamic, i.e., electron-density dependent, homonuclear coefficients $C_{9_{III}}$ and $\alpha_{0,I}$ in Eq. (7) for an atom in a molecule as

$$C_{9_{III}}[n(\mathbf{r})] \approx \left(\frac{V_I[n(\mathbf{r})]}{V_I^{\text{free}}[n^{\text{free}}(\mathbf{r})]} \right)^3 C_{9_{III}}^{\text{free}}, \tag{8}$$

$$\alpha_{0,I}[n(\mathbf{r})] \approx \left(\frac{V_I[n(\mathbf{r})]}{V_I^{\text{free}}[n^{\text{free}}(\mathbf{r})]} \right) \alpha_{0,I}^{\text{free}}, \tag{9}$$

V_I^{free} and V_I representing the atomic volume of the free atom and of the atom in the molecule, respectively. An analogous approximation to the C_6 coefficient has been shown to be accurate within 5% compared to experimental data for a wide range of molecules.[36]

The reference free-atom $C_{9_{III}}^{\text{free}}$ coefficients have been calculated according to Eq. (5) and using the frequency-dependent polarizability data obtained by Chu and Dalgarno[45] who relied on self-interaction corrected time-dependent DFT. Furthermore, they scaled the static polarizability to reproduce experimental or high-level many-body quantum electrodynamics calculations, leading to $C_{6_{II}}^{\text{free}}$ coefficients of nonmetallic elements with only 3% averaged deviation from experiment. Due to the triple product of polarizability in Eq. (5), slightly larger errors ($\approx$5%) are found for the $C_{9_{III}}$ coefficients.

The volume ratio in Eq. (8) is computed according to Hirshfeld volume partitioning[46,47] of an atom in a molecule,

$$\frac{V_I[n(\mathbf{r})]}{V_I^{\text{free}}[n^{\text{free}}(\mathbf{r})]} = \left(\frac{\int d\mathbf{r} \, r^3 n_I(\mathbf{r})}{\int d\mathbf{r} \, r^3 n_I^{\text{free}}(\mathbf{r})} \right), \tag{10}$$

where r is the distance from atom I, and $n_I(\mathbf{r})$ is the *effective* electron density of atom I in a molecule with electron density

$n(\mathbf{r})$: $n_I(\mathbf{r}) = n_I^{\text{free}}(\mathbf{r}) \cdot n(\mathbf{r}) / \Sigma_J n_J^{\text{free}}(\mathbf{r})$. The sum goes over all atoms J, positioned as in the molecule. It turns out that the volume ratio is fairly invariant with respect to the approximations made when computing the electronic structure. Unless stated otherwise, here we compute atomic and molecular electron densities using KS-DFT with the generalized gradient approximated functional PBE.[48]

C. Damping at short distances

Equations (2) and (3) are exact in the dissociative limit ($R_{IJ} \to \infty$). While the two-body dispersion energy is known[49] to converge to a finite attractive value in the limit of $R_{IJ} \to 0$ it is less obvious how to interpolate two- and three-body interatomic contributions at equilibrium geometries. Within the usual two-body C_6 correction schemes, empirical damping functions are used to this end as a smooth switch.[50–53] For the dispersion interaction energy between two hydrogen atoms, however, Koide, Meath, and co-workers[54] derived an analytical damping function that takes the form of an incomplete gamma function. Here, we use the corresponding simplification thereof, as proposed by Tang and Toennies.[6,37]

$$f_6^d(R_{IJ}) = 1 - e^{-b_{IJ}R_{IJ}} \sum_{k=0}^{n=6} \frac{(b_{IJ}R_{IJ})^k}{k!}, \tag{11}$$

where b is a range parameter that reflects the size of the atom pair, IJ. Interatomic potentials based on this damping function yielded CCSD(T) quality predictions for rare gas and mercury dimers.[7,55] This approach has also been leveraged for the accurate prediction of intermolecular dispersion energies within dispersion-corrected Møller–Plesset second-order perturbation theory.[56] The physical justification for the accuracy of the TT damping function for atoms other than hydrogen or rare gases is provided by the law of corresponding states. Note that the choice of the damping strongly affects quantitative estimates of dispersion contributions not only for short interatomic distances but also for equilibrium geometries. Since the TT damping has been derived from results for spherical atoms, we consider it to represent the least approximate way of damping. Our comparison to SAPT dispersion energy results (see below) empirically justifies this choice.

Correlation of rare gas dimers suggests a linear dependence of the range parameter b_{IJ} on D_{IJ}, the sum of atomic vdW radii of atoms I and J (see Fig. 2), $b_{IJ} = -0.33 D_{IJ} + 4.39$ bohr^{-1}. Such a linear relationship was already proposed by Meath and co-workers,[54] and here we confirm this idea for a large and consistent database of interatomic pairs. We define b for any rare gas dimer from the sum of its atomic vdW radii as extracted from the scaled atomic volume in a molecule [Eq. (10)]. The required free atom vdW radii have been obtained from coupled-cluster calculations of the free atom electron density.[36]

In order to damp the C_9 term, we adapt the aforementioned scheme by assuming that a triple product of two-body damping functions can be used,

$$f_{\text{ATM}}^d(R_I, R_J, R_K) = f_6'(R_{IJ}) \times f_6'(R_{IK}) \times f_6'(R_{JK}), \tag{12}$$
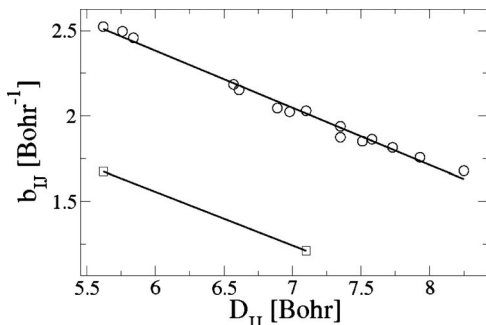
with

FIG. 2. Correlation of sum of rare gas atomic vdW radii, D_{IJ}, with range parameters b_{IJ} and b'_{IJ} in the TT damping function for two-body (circle) and three-body (square) terms, respectively. Linear regression for two-body: $b_{IJ} = -0.33 \times D_{IJ} + 4.39$ Bohr^{-1}, and interpolation for three-body: $b'_{IJ} = -0.31 \times D_{IJ} + 3.43$ Bohr^{-1}. Regression data from Ref. 6 and interpolation data from Refs. 57 and 58.

$$f'_6(R_{IJ}) = 1 - e^{-b'_{IJ}R_{IJ}} \sum_{k=0}^{n=6} \frac{(b'_{IJ}R_{IJ})^k}{k!}. \qquad (13)$$

Szalewicz and co-workers found this assumption to be accurate for the He and Ar trimer. We continue to build on their results by interpolating, in analogy to the two-body case, the three-body range parameters b'_{IJ} as a function of D_{IJ} for these two trimers.[57,58] This interpolation is also shown in Fig. 2, $b'_{IJ} = -0.31 D_{IJ} + 3.43$ bohr^{-1}. We note that the slope of the (correlated) two- and (interpolated) three-body range parameters is similar. Due to a samller value of the intercept, however, the three-body dispersion is damped more rapidly than the two-body term for decreasing distances. A qualitative illustration of the damped three-body energy as a function of the angle for an isosceles triangle is given in Fig. 1. Note that in the remainder of this study, we shall denote sums over damped interatomic C_6 and C_9 energy terms in Eqs. (2) and (3) collectively as $E^{(2)}$ and $E^{(3)}$, respectively.

III. BENCHMARK OF C_9, $E^{(2)}$, AND $E^{(3)}$

In order to benchmark the above outlined scheme for C_9 coefficients we used the dipole oscillator strength distribution (DOSD) reference database of Meath and co-workers.[59–72] It includes pseudo-DOSD data for 49 atoms and molecules, allowing the calculation of 18 424 intermolecular and interatomic reference C_9 coefficients. The accuracy of pseudo-DOSD C_6 and C_9 coefficients is limited only by the quality of experimental dipole oscillator strength data and they were shown to be accurate within 2%–3%, as illustrated by comparison between different sets of experimental data.[59–72] We calculated intermolecular dispersion coefficients as a sum over the corresponding interatomic C_6 and C_9 coefficients [see Eq. (8) and Ref. 36]. Geometries of all molecules in the database were optimized with the PBE (Ref. 48) functional using DFT calculations in the FHI-AIMS (Ref. 73) computer code. Our scheme yields a mean absolute error of 7.2% with respect to 18 424 reference pseudo-DOSD C_9 coefficients. Such an accuracy is similar to previously obtained molecular C_6 coefficients.[36] A slightly larger error for C_9 coefficients (7.2% versus 4.5% for C_6) is commensurate with the aforementioned larger errors obtained for the free-atom

C_{9III} coefficients calculated from frequency-dependent polarizabilities of Chu and Dalgarno.[45]

We performed additional testing of the accuracy of interatomic $E^{(2)}$ and $E^{(3)}$ energies by comparing to SAPT results for $\pi-\pi$ interacting dimer potential energy surface of benzene (491 dimer geometries),[38] and B-DNA structures (ten geometries).[39] For all the 491 geometries, our $E^{(2)}$ and $E^{(2)} + E^{(3)}$ contributions never exceed 100% of the SAPT dispersion energy. On average, the interatomic C_6 terms yield 73% of the benzene dimer SAPT results, adding the overall repulsive C_9 terms reduces this value to 70%. In the case of the DNA structures, we recover 77% and 66% for the $E^{(2)}$ and $E^{(2)} + E^{(3)}$ contributions, respectively. These findings are consistent with literature estimates for small molecular dimers where the higher-order two-body C_8 and C_{10} contributions to the attractive dispersion energy still account for 30%–40%.[47]

IV. RESULTS

A. Computational details

For the remainder of this study all the C_6 and C_9 calculations have been carried out for fixed geometries using the FHI-AIMS (Ref. 73) computer code with the PBE functional. In the case of DHFR and DNA, the fixed averaged C_6 and C_9 coefficients from Table I have been used. All calculation parameters (k-points and basis sets) were converged with respect to atomic volume ratio in Eq. (10).

All molecular figure pictures have been generated using the program VMD,[74] the molecular crystal figures have been generated using the program GDIS.[75] We also reiterate that, in the remainder of this study, we shall denote sums over damped interatomic C_6 and C_9 energy terms in Eqs. (2) and (3) collectively as $E^{(2)}$ and $E^{(3)}$, respectively.

B. Dispersion coefficients

Atomic dispersion coefficients C_6, C_9, vdW radii, and polarizabilities of free atoms H, He, C, N, O, F, Ne, Si, P, S, Cl, Ar, Br, and Kr feature in Table I. These coefficients have been obtained by numerical integration according to Eqs. (4) and (5) and using the frequency-dependent polarizability data of Chu and Dalgarno.[45] Both dispersion coefficients reflect the usual trends of the periodic table, as one goes to the right in a period, they decrease, same as polarizability, as one goes down, they increase. In order to also illustrate the impact of placing atoms into molecules, typical C_9 and C_6 coefficients of hybridized atoms are also enlisted; the change within a given row is most pronounced for carbon and silicon.

Furthermore, for carbon and oxygen the variation in electronic configuration/hybridization affects both coefficients. They decrease as one goes from sp to sp^2 to sp^3. Clearly, the meaning of this observation is that due to the increasing number of covalently bonded neighbors, as sp turns into sp^3, atomic polarizability, and thereby dispersion coefficients, decrease.

TABLE I. Computed C_6 and C_9 coefficients in (Hartree Bohr^6) and (Hartree Bohr^9), respectively. Atomic polarizabilities (Bohr^3) and atomic vdW radii (bohr). Atomic polarizabilities correspond to static values of frequency dependent polarizabilities in Ref. 45, scaled by volume for hybridized atoms in molecules. Hybridized values are averaged over molecules in the DOSD database. The vdW radii are computed using atomic CCSD electron density as explained in Ref. 36. Superscripts s, sp^2, and sp^3 denote atomic hybridization states.

Atom	α	C_6	C_9	R_{vdW}
H^{free}	4.50	6.5	21.6	3.10
H^s	2.75	2.42	4.91	2.63
He	1.38	1.46	1.47	2.65
C^{free}	12.0	46.6	373	3.59
C^{sp}	9.73	30.6	199	3.35
C$^{sp^2}$	9.67	30.3	195	3.34
C$^{sp^3}$	8.64	24.1	139	3.22
N^{free}	7.40	24.2	117	3.34
N$^{sp^2,sp^3}$	6.36	17.9	74.4	3.18
O^{free}	5.40	15.6	52.6	3.19
O$^{sp^2}$	4.92	13.0	39.8	3.09
O$^{sp^3}$	4.81	12.4	37.1	3.07
F^{free}	3.80	9.52	24.2	3.04
F$^{sp^3}$	3.46	7.89	18.3	2.95
Ne^{free}	2.67	6.38	12.0	2.91
Si^{free}	37.0	305	8550	4.20
Si$^{sp^3}$	25.6	146	2846	3.72
P^{free}	25.0	185	3561	4.01
S^{free}	19.6	134	1925	3.86
S$^{sp^3}$	18.2	115	1532	3.76
Cl^{free}	15.0	94.6	1014	3.71
Cl$^{sp^3}$	14.6	89.4	932	3.68
Ar	11.1	64.3	518	3.55
Br^{free}	20.0	162	2511	3.93
Br$^{sp^3}$	19.5	155	2340	3.90
Kr	16.8	130	1572	3.82

TABLE II. Interatomic $E^{(2)}$ and $E^{(3)}$ contributions to S22 benchmark data set results in kcal/mol. CCSD(T) results from S22 data set in Ref. 9.

No.		$E^{(2)}$	$E^{(3)}$	CCSD(T)
1	(NH$_3$) dimer (C$_{2h}$)	−1.43	0.00	−3.17
2	(H$_2$O) dimer (C$_s$)	−1.80	−0.01	−5.02
3	Formic acid dimer	−7.87	0.02	−18.61
4	Formamide dimer (C$_{2h}$)	−5.69	0.02	−15.96
5	Uracil dimer (C$_{2h}$)	−7.03	−0.07	−20.65
6	2-pyridoxine-2-aminopyridine (C$_1$)	−7.16	−0.02	−16.71
7	Adenine-thymine WC	−7.54	−0.04	−16.37
8	(CH$_4$) dimer (D$_{3d}$)	−0.68	0.02	−0.53
9	(C$_2$H$_4$) dimer (D$_{2d}$)	−1.96	0.05	−1.51
10	Benzene-CH$_4$ (C$_3$)	−1.97	0.14	−1.50
11	Benzene dimer (C$_{2h}$)	−5.64	0.68	−2.73
12	Pyrazine dimer (C$_s$)	−5.92	0.60	−4.42
13	Uracil dimer (C$_2$)	−8.90	0.96	−10.12
14	Indole-benzene (C$_1$)	−8.48	1.10	−5.22
15	Adenine-thymine stack	−13.04	1.54	−12.23
16	Ethene-ethine (C$_{2v}$)	−0.93	0.01	−1.53
17	Benzene-H$_2$O (C$_s$)	−2.35	0.15	−3.28
18	Benzene-NH$_3$ (C$_s$)	−2.15	0.14	−2.35
19	Benzene-HCN (C$_s$)	−2.84	0.15	−4.46
20	Benzene dimer (C$_{2v}$)	−3.61	0.21	−2.74
21	Indole-benzene T-shape	−5.24	0.30	−5.73
22	Phenol dimer (C$_1$)	−5.18	0.19	−7.05

C. S22 data set

Interatomic C_6 and C_9 contributions to dimer interaction energies of the S22 benchmark data set[9] feature in Table II. This data set contains a representative sample of vdW and hydrogen bonded molecular dimers, and is frequently used for benchmarking vdW corrections. Note that the total magnitude of the two-body dispersion energies can be of the same order as the binding energy, in the case of benzene dimer even twice as large. This result is consistent with perturbational analysis of intermolecular energies according to SAPT.[38] Note that at equilibrium distance the attractive terms, including two-body dispersion energies, are counterbalanced by all repulsive terms, such as Pauli repulsion or three-body dispersion energy. This explains why the attractive dispersion energy can be *larger* than the total binding energy and highlights the importance of an accurate treatment of the former.

As one would expect for isolated and small to medium-sized molecular dimer cases the three-body dispersion contribution is mostly rather small. However, in some cases such as stacked adenine-thymine or indole-benzene the C_9 contribution is significant, reaching 10% or 20% of the total binding energy, respectively. This differing behavior can be un-

derstood when considering the particular geometry of the π-π interacting systems. Figure 3 depicts the indole-benzene geometry. There are many configurations corresponding to repulsive triangular triplets across the two molecules ($\phi \leq 2\pi/3$), and fewer attractive configurations ($2\pi/3 \leq \phi \leq 4\pi/3$). Furthermore, for some dimers in this data set, the C_9 contribution is negligible simply because the molecules are too small to exhibit any triplet that is not attenuated by the damping function.

D. Bulky systems

For a variety of bulky systems, i.e., macromolecular or condensed phase systems, Table III features estimates of $E^{(2)}$ and $E^{(3)}$ contributions, together with relevant energies such as binding or cohesive energies.
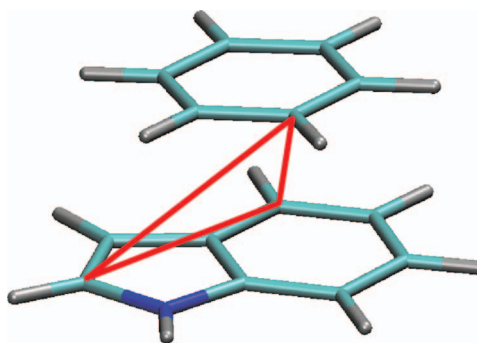

FIG. 3. Indole/C$_6$H$_6$ structure in S22 data set used to estimate two- and three-body interatomic dispersion contribution. The red lines illustrate one of all the atomic triplets that are at the origin of a repulsive intermolecular three-body contribution.

TABLE III. Estimates of leading two- and three-body dispersion energy contributions to cohesive, binding, and folding energies E, respectively. All values are in kcal/mol.

System	$E^{(2)}$	$E^{(3)}$	E
Crystals			
Ar crystal	−2.17	0.07	−2.03[a]
Benzene crystal	−16.1	1.67	−10.6[b]
Diamond	−50.5	2.03	−171.3[c]
Ice Ih	−2.96	0.04	−14.1[d]
Carbon materials			
Bigraphene	−2.30	0.61	−1.20[e]
$(C_{60})_2$	−11.4	1.02	−7.33[f]
Biomolecules			
Drug (ellipticine)	−57.0	8.90	−37.0[g]
$Ala_{10}(\alpha\text{-FES})$/residue	−5.95	0.44	−0.96[h]
DHFR/amino acid[i]	−74.8	2.8	⋯
DNA/base[i]	−130.9	5.8	⋯

[a]Cohesive energy, experimental, and theoretical from Refs. 27, 76, and 77, respectively.
[b]Cohesive energy/molecule experimental result from Ref. 78.
[c]Experimental cohesive energy per atom pair from Ref. 79 and references therein.
[d]Experimental low temperature (10 K) lattice energy per molecule from Ref. 80, structure relaxed with PBE from Ref. 81.
[e]Binding energy derived from exfoliation of finite graphene flakes from Ref. 82.
[f]Experimental fullerene interaction energy from Ref. 83.
[g]Theoretical interaction energy from Ref. 84.
[h]Theoretical energy difference between elongated planar backbone and α-helical folded conformers, using PBE+C_6 (Ref. 36).
[i]Averaged residual contributions to unknown total energies, made for fixed C_6- and C_9-values from Table I.

1. Crystals

For the Ar crystal, the three-body estimate amounts to less than 5%, which compares well to the total many-body contribution of 6.6% in Ref. 22. However, using the same level of theory we predict more than 15% for the molecular benzene crystal. Using SAPT(DFT), Podeszwa and Szalewicz[85] calculated an intermolecular three-body dispersion contribution for the cyclic benzene trimer in crystal structure geometries of 0.18 kcal/mol. For the same trimer, the corresponding intermolecular C_9 term by summing over all those triplets that involve one atom per molecule amounts to 0.14 kcal/mol, in good agreement with the work of Podeszwa and Szalewicz. On the other hand, the total interatomic C_9 contribution to the three-body energy in the benzene trimer is 0.89 kcal/mol. This analysis reveals that the large relative C_9 contribution of 15% to the cohesive energy of the benzene crystal is dominated by three-body summations involving benzene dimers.

By contrast, $E^{(3)}$ contributes only slightly more than 1% to the cohesive energy in the diamond crystal. This is not surprising since this energy is dominated by strong covalent bonds. The $E^{(2)}$ contribution is more surprising in this case. However, one can speculate if this result is real, or rather due to insufficient damping at short covalent bond distances, or due to the neglect of the dynamic screening of long range dispersion interactions. In Ref. 86, van der Waals contributions to the cohesive energy of the silicon crystal (exhibiting

the same crystal structure) were estimated to reach up to 10%. We also note that the $E^{(3)}/E^{(2)}$ ratio reduces from 10% to 4% when going from benzene to diamond crystal.

In the case of ice-Ih the $E^{(3)}$ contribution is nearly negligible; we note that the $E^{(2)}$ contribution in ice is likewise rather small when compared to its relative contribution to cohesive energies in the other molecular crystals. This finding suggests that the considerable cooperativity found for water clusters[87] has other origins than dispersion.[88]

2. Carbon materials

We investigated the fullerene dimer and bilayer graphene as representative model systems for aromatic carbon nanomaterials. For these two examples, the C_9 contributions reach remarkable magnitudes, namely, 14% and 51%. We reiterate that these terms correspond to interatomic potentials and do not represent three-body terms in the sense of intermolecular interaction perturbation theory. Furthermore, the higher order interatomic terms might counteract this effect. In addition, one may argue about the accuracy of the damping function. However, especially in the bilayer graphene case, a significant part of the repulsive three-body contribution comes from distances beyond the influence of the damping function. At such distances, it is reasonable to expect the Axilrod–Teller–Muto term to yield an accurate representation of the three-body dispersion energy.

3. Biomolecules

Current flavors of force-field based biomolecular simulation do not dispose of many-body dispersion terms. At most, many-body contributions due to induction are introduced via empirical polarizability. See Ref. 89 and references therein. Predicting accurate biomolecular noncovalent interaction energies to compare ligand candidates is a crucial component in drug design that relies on force field docking tools for screening,[90,91] or more efficient first principles rational compound design approaches.[92–94]

The potential energy of interaction between DNA and the intercalator drug ellipticine has recently been estimated to amount to ∼37 kcal/mol.[84] We find that the corresponding two- and three-body dispersion energies amount to considerable −57.0 and 8.9 kcal/mol, respectively. The intercalated drug in Fig. 4 illustrates the large number of atomic pairs and triplets at typical vdW distances resulting in such large energy contributions.

The $E^{(3)}$ contribution to the potential energy difference per residue between folded and elongated polyalanine decamer (Ala_{10}) amounts to 46%. This is mainly due to a very small energy difference between α-helical and fully extended geometries due to the formed macrodipole in the former structure. However, this example highlights the importance of an accurate description of many-body dispersion to achieve the "chemical accuracy" (1 kcal/mol) also in biological systems.

The macromolecular DHFR and DNA systems, depicted in Fig. 4, pose convergence problems in electronic structure calculations, prohibiting straightforward evaluation of dynamic dispersion coefficients. We have therefore estimated
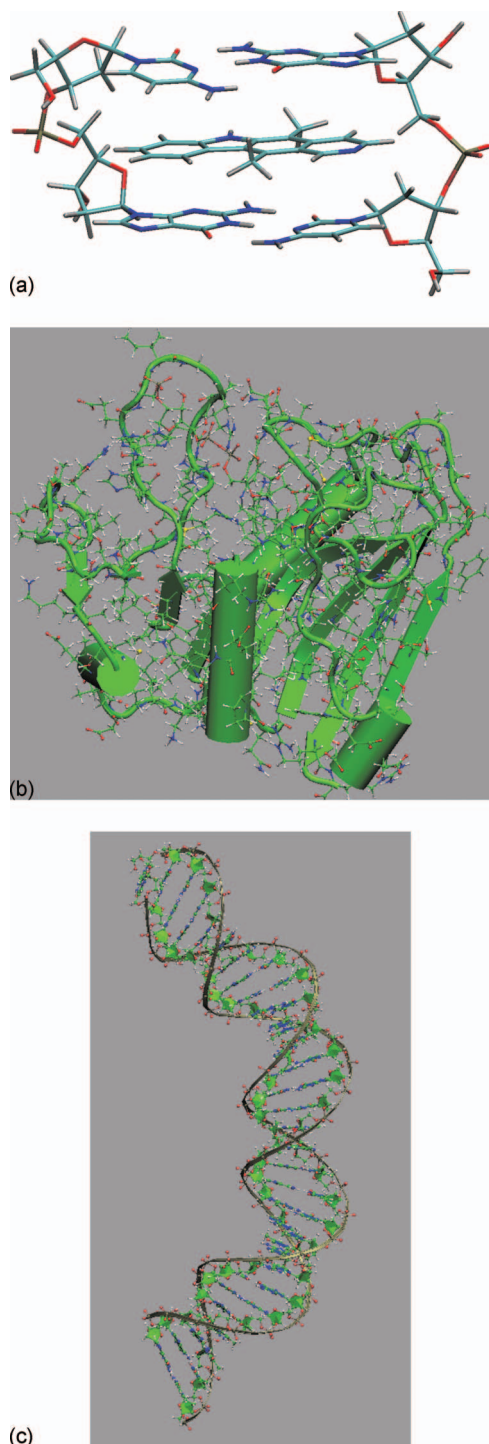
(a)

(b)

(c)

FIG. 4. Pictures of investigated ellipticine drug intercalated in DNA model according to Ref. 84, DHFR, and DNA structures. For fixed geometries these systems have been used to estimate two- and three-body interatomic dispersion energy contributions in Table III.

averaged residual $E^{(2)}$ and $E^{(3)}$ contributions to total energies of these two systems using constant typical coefficients from Table I. The DNA structure corresponds to a test system in the latest distribution of the visualization package VMD,[74] the DHFR protein structures have been downloaded from the protein data bank. To avoid counting the intraresidue covalent bonding contributions for these two systems, we estimated the $E^{(2)}$ and $E^{(3)}$ energies in the following way:

$$E^{(2)} = \frac{1}{N}\sum_n (E^{(2),\text{full}} - E^{(2),\text{full}-n} - E^{(2),n}), \quad (14)$$

where "full" signifies the full system and "full$-n$" means the full system without residue n, all geometries being frozen. The index n runs over all residues (amino acids or base pairs). The $E^{(3)}$ energy is calculated using the same formula. The two-body contribution is still significant even after removal of the intraresidue covalent bonds, however, the values are reasonable if we compare them to the purely intermolecular $E^{(2)}$ energy for the drug-DNA binding. One should also note that some part of $E^{(2)}$ and $E^{(3)}$ for DHFR and DNA is due to the *backbone-residue* covalent bonds. As such these estimates give only a vague idea of the order of magnitude for these systems. The three-body estimates of ~3 kcal/mol per residue for DHFR and ~6 kcal/mol per base pair for double-stranded DNA are far from being negligible, however. These numbers are evidently too large to be neglected while still aiming to achieve "chemical accuracy": the level of accuracy ideally realized within truly predictive atomistic simulation methods.

E. Energy ranking

In Sec. IV D, numerical estimates of the energetic contributions due to two- and three-body dispersion effects have been provided. While for some systems the relative three-body contributions can be substantial (carbon materials, biomolecules), for other systems they are very small (ice, diamond). In this section, we investigate systems where these many-body contributions might affect trends, i.e., the qualitative outcome of predicted energy rankings. Specifically, we studied intermolecular energies of 42 DNA base pairs, as well as relative cohesive energies among polymorphs of four different molecular crystals.

1. Ranking of base pair interactions

Table IV features state-of-the-art coupled-cluster intermolecular binding energies and two- and three-body contributions for 42 selected inter- and intrastrand DNA base pairs, as published in the JSCH-2005 database.[9] We have used this data to reveal the effect of the three-body dispersion contribution on the ranking of intermolecular energies by testing if the ranking of intermolecular energies is altered when three-body dispersion contributions are being neglected. The three-body term can reach up to 1.4 kcal/mol, a substantial contribution when compared to intermolecular energies that range from -11 to 5 kcal/mol. If we assume that the $E^{(3)}$ term due to C_9 is the dominating many-body dispersion contribution, subtracting $E^{(3)}$ from the CCSD(T) estimates will evidence the impact of $E^{(3)}$ on the ranking. To this end, $E^{(3)}$ has been subtracted from the CCSD(T) estimates, and the entries in Table IV are ranked according to that difference. The results in Table IV clearly demonstrate that the ranking of base pairs does alter on occasion depending on if three-body dispersion forces have been taken into account or not. The overall ordering of the CCSD(T) energies, however, is rather conserved.

TABLE IV. Computed two-body dispersion $E^{(2)}$ and three-body dispersion $E^{(3)}$ contributions to intermolecular energies of selected stacked and intrastrand base pairs from the JSCH-2005 database (Ref. 9) in kcal/mol. The column O indicates the order when ranked according to the coupled cluster interaction energy (CC-column) from Ref. 9. The systems have been ranked according to the CC-$E^{(3)}$-column: CC interaction energies without three-body dispersion contribution.

System	$E^{(2)}$	$E^{(3)}$	CC-$E^{(3)}$	O	CC
GUst	−9.72	1.16	−11.94	1	−10.78
GGst	−11.23	1.40	−11.94	2	−10.54
CUst	−8.01	0.90	−10.64	3	−9.74
GCst	−8.96	1.07	−10.27	4	−9.2
GAst	−10.71	1.33	−10.09	7	−8.76
CCst	−8.18	0.94	−9.98	5	−9.04
CC4	−8.43	0.96	−9.77	6	−8.81
CC11	−7.92	0.88	−9.45	8	−8.57
ACst	−9.28	1.11	−9.35	10	−8.24
CC14	−8.55	0.96	−9.18	11	−8.22
CC8	−7.22	0.77	−9.16	9	−8.39
AUst	−9.46	1.14	−9.12	12	−7.98
CC9	−8.43	0.99	−8.9	13	−7.91
CC3	−8.55	0.96	−8.73	15	−7.77
CC13	−6.84	0.76	−8.65	14	−7.89
GA_AG	−11.78	1.47	−8.14	19	−6.67
CC10	−7.99	0.92	−8.07	18	−7.15
CG0_GC	−6.62	0.60	−7.79	17	−7.19
CC12	−4.50	0.38	−7.69	16	−7.31
UUst	−7.23	0.82	−7.24	20	−6.42
AAst	−10.02	1.23	−6.99	21	−5.76
AG_AG	−8.64	1.06	−6.75	22	−5.69
TA08_AT	−13.40	1.50	−6.55	24	−5.05
AT10_AT	−9.27	1.13	−6.17	25	−5.04
AG_TC	−6.79	0.76	−6.1	23	−5.34
TG_TG	−6.70	0.63	−5.47	26	−4.84
AA0_AA	−10.04	1.18	−5.09	27	−3.91
GT10_AC	−8.82	1.05	−4.86	28	−3.81
AA20_AA	−10.63	1.29	−4.81	30	−3.52
TG_AC	−7.47	0.74	−4.54	29	−3.8
GT10_TG	−10.66	1.26	−4.44	31	−3.18
AA0_TT	−9.32	0.99	−3.56	33	−2.57
CC2	−8.50	0.99	−3.29	34	−2.3
AA20_TT	−2.23	0.03	−2.92	32	−2.89
GG0_GG	−6.08	0.67	−2.11	35	−1.44
GG0_CC	−0.82	0.04	−0.61	36	−0.57
CC7	−5.14	0.51	−0.49	37	0.02
GA_TC	−6.97	0.80	0.25	38	1.05
CC5	−8.08	0.91	1.25	39	2.16
CC6	−8.24	0.94	1.58	40	2.52
CC1	−7.66	0.91	3.41	41	4.32
GC0_GC	−10.43	1.24	3.43	42	4.67

We used the results in Table IV to elucidate another aspect, namely, the relationship between $E^{(3)}$ and $E^{(2)}$. For these DNA base pair structures, a clear correlation exists between these two energy contributions, $E^{(3)} = (-0.14 \times E^{(2)}) - 0.19$ kcal/mol, with correlation coefficient $r = 0.986$ (see Fig. 5). If this correlation proved to be transferable one could effectively estimate the more complicated three-body contributions via the two-body terms.

2. Molecular crystals

Polymorphism of molecular crystal structures plays a major role in pharmaceutical considerations of drug candidates.[95] In Ref. 96, Neumann *et al.* recently succeeded to predict from first principles the experimentally determined most stable polymorphs of four different molecular crystals set forth within the fourth crystal structure blind test.[40] To this end they developed a force-field approach based on DFT combined with C_6 corrections[97] using the PW91 exchange-correlation functional.[98,99] Geometries and unit cells of said four crystals are displayed in Fig. 6. Functional groups that feature in this set of molecules include aromatic cores, flexible alkyl chains, nitrogen, and sulfur atoms in differing hybridization states, as well as halogens. Within our approach, the presence of different atomic environments leads to
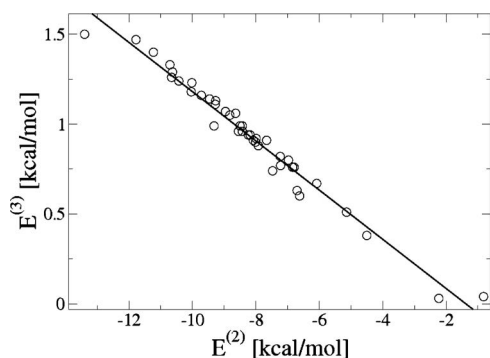
FIG. 5. Correlation of two- and three-body dispersion energy contributions to DNA base pair intermolecular energies displayed in Table IV, $E^{(3)} = -0.14 \times E^{(2)} - 0.19$ kcal/mol. Correlation coefficient: 0.986.

changes in the effective dispersion coefficients. For example, the resulting C_6 coefficients range from 30 to 39 for carbon, 91 to 100 for sulfur, and 17 to 19 Hartree Bohr^6 for nitrogen.

Our two- and three-body energy contributions to relative cohesive energies per molecule are given in Table V, together with cohesive energies according to DFT+C_6 estimates from Ref. 96, or according to the PBE+vdW method of Ref. 36 computed for this study. Both dispersion corrected DFT methods predict the same polymorph to be the most stable for all four crystals. However, they yield differing results, up to half a kcal/mol, when comparing polymorphs 2 or 3. It is difficult to tell if this is mainly due to the exchange-correlation functional, to the differing definition of
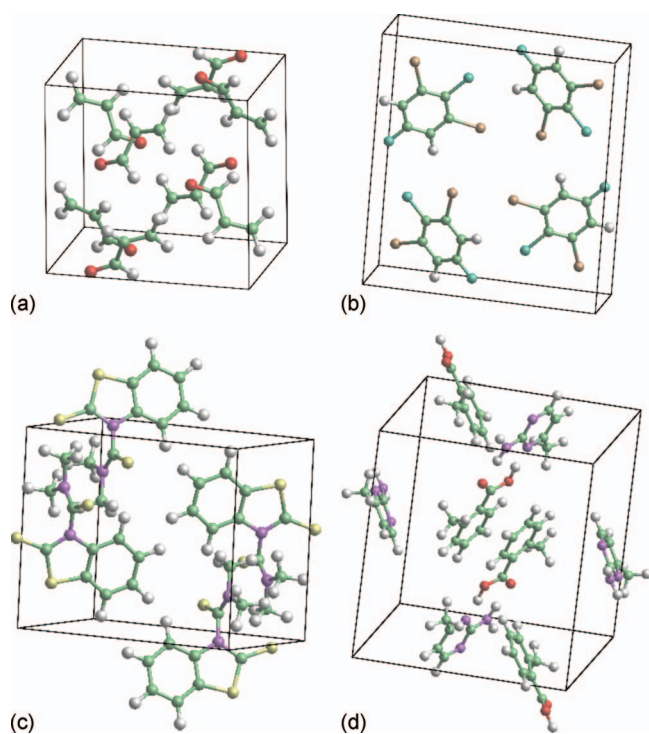

FIG. 6. Structures of the most stable polymorphs in Table V. Molecules XII (top, left), XI (top, right), XIV (bottom, left), and XV (bottom, right). Red denotes oxygen, green carbon, white hydrogen, orange bromine, turquoise chlorine (in between bromine) and fluorine (para with respect to chlorine), violet nitrogen, and yellow sulfur.

TABLE V. Relative cohesive energies per molecule in kcal/mol according to the molecular crystal structure blind test 2007 (Ref. 40). Polymorph structures and PW91+vdW were published in Ref. 96. Geometries and unit cells of the most stable polymorphs (1) are shown in Fig. 6.

No. of polymorph	PW91+vdW [a]	PBE+vdW [b]	$E^{(2)}$	$E^{(3)}$
		XII		
1	0.0	0.0	0.0	0.0
2	0.28	0.58	1.66	−0.07
3	0.47	0.40	−1.07	0.06
		XI		
1	0.0	0.0	0.0	0.0
2	0.32	0.59	0.70	−0.09
3	0.34	0.88	1.77	−0.21
		XIV		
1	0.0	0.0	0.0	0.0
2	0.47	1.05	1.94	−0.32
3	1.05	0.98	1.25	−0.13
		XV		
1	0.0	0.0	0.0	0.0
2	0.50	0.35	1.54	0.02
3	0.59	0.75	2.72	−0.14

[a]Constant C_6 corrected DFT results from Ref. 97.
[b]Computed with dynamic C_6 corrected DFT described in Ref. 36.

C_6 and vdW radii (one being constant, the other being dynamic), or to the choice of the damping function.

Inspection of the two- and three-body contributions in Table V makes clear that the most stable polymorph has the largest attractive $E^{(2)}$ as well as the largest repulsive $E^{(3)}$. Note that both of these contributions are at least of a similar order of magnitude as the cohesive energy differences between the polymorphs. Adding the three-body contribution to the cohesive energy can alter the ranking between polymorphs 2 and 3 for crystals XI and XIV.

V. DISCUSSION

Conventionally, many atomistic force fields assume that many-body dispersion terms can be effectively incorporated in the Lennard-Jones type of potentials.[89] Our results are relevant in this context, possibly for the construction of more sophisticated effective two- and three-body interatomic potential models that explicitly include not only many-body induction but also dispersion effects. In this context, the scheme presented here promises to be particularly useful to further the development of automated force field optimization approaches, such as in Ref. 100, toward more sophisticated potentials that are capable to deal with real systems. For example, one could envision the parametrized dynamic determination of atomic volumes within reactive force field simulations, or exploiting links to polarizable force fields,[101,102] or force fields with variable polarizabilities.

Furthermore, the presented scheme might prove helpful for developing interatomic dispersion corrections to electronic structure theory. The accuracy of DFT, for example, depends greatly on the deployed approximation to the exchange-correlation potential (v_{xc}), and on the system and properties that are being studied.[103] The difficulties to obtain

a reasonable DFT based description of van der Waals interactions are well recognized.[104–106] To superimpose a dissociative pairwise interatomic London potential decaying as R^{-6} constitutes one of the simplest but most effective remedies for this inaccuracy.[107,108] Today a broad range of implementations has been designed and used for many systems.[36,50,52,53,109–114] An extension in the sense of DFT $+E^{(2)}+E^{(3)}$ could lead to increasingly accurate predictions, once damping functions are devised that appropriately negotiate the combination with a given functional. Recently we realized that nonempirical (semi-) local functionals do not appear to be suitable for such a scheme.[21,22] A DFT$+E^{(2)}$ $+E^{(3)}$ approach should be particularly accurate if the DFT functional accounts for the correct interatomic short range energetics in the regime of orbital overlap.

VI. CONCLUSIONS

We extended, and assessed, the dynamic dispersion coefficient calculation methodology presented in Ref. 36 for computing the long range triple dipole C_9 terms that enter the Axilrod-Teller-Muto expression[25,26] for the three-body dispersion energy. The average deviation of computed C_9 coefficients from C_9 coefficients obtained using experimental DOSD data is 7.2%.

For interatomic short ranges, we adapted the TT scheme to consistently damp two- and three-body dispersion energies. The required damping range parameters, b_{IJ}, have been obtained as functions of vdW radii using a correlation for rare gas dimer and an interpolation for rare gas trimer data, respectively. We noted that the slope of the correlation is very similar to the slope of the interpolation.

For 491 geometries of the benzene dimer and ten different DNA base pair dimers, we found $E^{(2)}$ and $E^{(3)}$ contributions that are consistently smaller than available corresponding SAPT data for the full dispersion energy from literature. We expect that adding higher order pairwise terms, C_8 and C_{10}, will bring $E^{(2)}+E^{(3)}$ in better agreement with the SAPT predictions.

We presented a comprehensive table of C_6 and C_9 values for free atoms and atoms in molecules. Neglecting on-the-fly effects of these coefficients, they can serve as parameters in effective interatomic potentials that account for atom pairwise as well as nonadditive dispersion energies.

For various systems we estimated the leading order two- and three-body dispersion contributions to binding or cohesive energies. Throughout the systems investigated, the two-body dispersion energies are always of similar magnitude or even larger than the considered energy. For large molecular and condensed systems also the three-body dispersion energies become significant.

We conclude that it remains questionable if it is reasonable to generally neglect three-body dispersion energies. For the binding energies of the fullerene dimer, the bilayer graphene, and the DNA-ellipticine complex, the $E^{(3)}$ contributions can reach remarkable magnitudes, namely, 14%, 51%, and 24%, respectively. However, also to the cohesive energy of the molecular benzene crystal, three-body dispersion forces contribute more than 15%. For 42 DNA base

pairs or competing molecular crystal morphologies we have shown that the neglect of three-body dispersion energies can affect the energetic ranking qualitatively.

[1] A. J. Stone, *The Theory of Intermolecular Forces* (Oxford University Press, New York, 1996).
[2] D. Wales, *Energy Landscapes: Applications to Clusters, Biomolecules and Glasses* (Cambridge University Press, Cambridge, 2003).
[3] V. A. Parsegian, *Van der Waals Forces. A Handbook for Biologists, Chemists, Engineers, and Physicists* (Cambridge University Press, Cambridge, 2006).
[4] J. N. Israelachvili, *Intermolecular and Surface Forces* (Academic, New York, 1985).
[5] I. G. Kaplan, *Intermolecular Interactions: Physical Picture, Computational Methods and Model Potentials* (Wiley, New York, 2006).
[6] K. T. Tang and J. P. Toennies, J. Chem. Phys. **118**, 4976 (2003).
[7] P. Slaviček, R. Kalus, P. Paska, I. Odvarkova, P. Hobza, and A. Malijevsky, J. Chem. Phys. **119**, 2102 (2003).
[8] V. F. Lotrich and K. Szalewicz, Phys. Rev. Lett. **79**, 1301 (1997).
[9] P. Jurečka, J. Šponer, J. Černý, and P. Hobza, Phys. Chem. Chem. Phys. **8**, 1985 (2006).
[10] M. O. Sinnokrot, E. F. Valeev, and C. D. Sherrill, J. Phys. Chem. A **108**, 10200 (2004).
[11] A. J. Misquitta, B. Jeziorski, and K. Szalewicz, Phys. Rev. Lett. **91**, 033201 (2003).
[12] J. Černý, M. Kabeláč, and P. Hobza, J. Am. Chem. Soc. **130**, 16055 (2008).
[13] R. Bukowski, K. Szalewicz, G. C. Groenenboom, and A. van der Avoird, Science **315**, 1249 (2007).
[14] J. Harl and G. Kresse, Phys. Rev. Lett. **103**, 056401 (2009).
[15] M. Rohlfing and T. Bredow, Phys. Rev. Lett. **101**, 266106 (2008).
[16] R. Podeszwa, B. M. Rice, and K. Szalewicz, Phys. Rev. Lett. **101**, 115503 (2008).
[17] D. Lu, Y. Li, D. Rocca, and G. Galli, Phys. Rev. Lett. **102**, 206411 (2009).
[18] X. Ren, P. Rinke, and M. Scheffler, Phys. Rev. B **80**, 045402 (2009).
[19] S. Grimme, J. Antony, S. Ehrlich, and H. Krieg, J. Chem. Phys. **132**, 154104 (2010).
[20] K. Szalewicz, R. Bukowski, and B. Jeziorski, *Theory and Applications of Computational Chemistry: The First Forty Years* (Elsevier, New York, 2005), Chap. 33, p. 919.
[21] K. A. Maerzke, G. Murdachaew, C. J. Mundy, G. K. Schenter, and J. I. Siepmann, J. Phys. Chem. A **113**, 2075 (2009).
[22] A. Tkatchenko and O. A. von Lilienfeld, Phys. Rev. B **78**, 045116 (2008).
[23] P. Hohenberg and W. Kohn, Phys. Rev. **136**, B864 (1964).
[24] W. Kohn and L. J. Sham, Phys. Rev. **140**, A1133 (1965).
[25] B. M. Axilrod and E. Teller, J. Chem. Phys. **11**, 299 (1943).
[26] Y. Muto, J. Phys.-Math. Soc. Japan **17**, 629 (1943).
[27] K. Rościszewski, B. Paulus, P. Fulde, and H. Stoll, Phys. Rev. B **62**, 5482 (2000).
[28] Y. S. Kim, Phys. Rev. A **11**, 796 (1975).
[29] Y. S. Kim, Phys. Rev. A **11**, 804 (1975).
[30] R. G. Gordon and Y. S. Kim, J. Chem. Phys. **56**, 3122 (1972).
[31] K. Rapcewicz and N. W. Ashcroft, Phys. Rev. B **44**, 4032 (1991).

[32] P. Loubeyre, Phys. Rev. B **37**, 5432 (1988).

[33] J. Antony, B. Brüske, and S. Grimme, Phys. Chem. Chem. Phys. **11**, 8440 (2009).

[34] W. Heitler and F. London, Z. Phys. **44**, 455 (1927).

[35] R. Eisenschitz and F. London, Z. Phys. **60**, 491 (1930).

[36] A. Tkatchenko and M. Scheffler, Phys. Rev. Lett. **102**, 073005 (2009).

[37] K. T. Tang and J. P. Toennies, J. Chem. Phys. **74**, 1148 (1981).

[38] R. Podeszwa, R. Bukowski, and K. Szalewicz, J. Phys. Chem. A **110**, 10345 (2006).

[39] A. Fiethen, G. Jansen, A. Hesselmann, and M. Schutz, J. Am. Chem. Soc. **130**, 1802 (2008).

[40] G. M. Day, T. G. Cooper, A. J. Cruz-Cabeza, K. E. Hejczyk, H. L. Ammon, S. X. M. Boerrigter, J. S. Tan, R. G. D. Valle, E. Venuti, J. Jose, S. R. Gadre, G. R. Desiraju, T. S. Thakur, B. P. van Eijck, J. C. Facelli, V. E. Bazterra, M. B. Ferraro, D. W. M. Hofmann, M. A. Neumann, F. J. J. Leusen, J. Kendrick, S. L. Price, A. J. Misquitta, P. G. Karamertzanis, G. W. A. Welch, H. A. Scheraga, Y. A. Arnautova, M. U. Schmidt, J. van de Streek, A. K. Wolf, and B. Schweizer, Acta Crystallogr., Sect. B: Struct. Sci. **65**, 107 (2009).

[41] J. J. Rehr, E. Zaremba, and W. Kohn, Phys. Rev. B **12**, 2062 (1975).

[42] H. B. G. Casimir and D. Polder, Phys. Rev. **73**, 360 (1948).

[43] K. T. Tang and M. Karplus, Phys. Rev. **171**, 70 (1968).

[44] K. T. Tang, Phys. Rev. **177**, 108 (1969).

[45] X. Chu and A. Dalgarno, J. Chem. Phys. **121**, 4083 (2004).

[46] E. R. Johnson and A. D. Becke, J. Chem. Phys. **123**, 024101 (2005).

[47] A. Olasz, K. Vanommeslaeghe, A. Krishtal, T. Veszpremi, C. V. Alsenoy, and P. Geerlings, J. Chem. Phys. **127**, 224105 (2007).

[48] J. P. Perdew, K. Burke, and M. Ernzerhof, Phys. Rev. Lett. **77**, 3865 (1996).

[49] A. Koide, J. Phys. B **9**, 3173 (1976).

[50] U. Zimmerli, M. Parrinello, and P. Koumoutsakos, J. Chem. Phys. **120**, 2693 (2004).

[51] S. Grimme, J. Comput. Chem. **27**, 1787 (2006).

[52] F. Ortmann, F. Bechstedt, and W. G. Schmidt, Phys. Rev. B **73**, 205101 (2006).

[53] Q. Wu and W. Yang, J. Chem. Phys. **116**, 515 (2002).

[54] A. K. Dham, A. R. Allnat, A. Koide, and W. J. Meath, Chem. Phys. **196**, 81 (1995).

[55] X. W. Sheng, P. Li, and K. T. Tang, J. Chem. Phys. **130**, 174310 (2009).

[56] A. Tkatchenko, R. A. DiStasio, Jr., M. Head-Gordon, and M. Scheffler, J. Chem. Phys. **131**, 094106 (2009).

[57] V. F. Lotrich and K. Szalewicz, J. Chem. Phys. **106**, 9688 (1997).

[58] W. Cencek, M. Jeziorska, O. Akin-Ojo, and K. Szalewicz, J. Phys. Chem. A **111**, 11311 (2007).

[59] R. Kumar and R. J. Meath, Mol. Phys. **106**, 1531 (2008).

[60] B. L. Jhanwar and W. J. Meath, Chem. Phys. **67**, 185 (1982).

[61] A. Kumar and W. J. Meath, Mol. Phys. **90**, 389 (1997).

[62] G. D. Zeiss, W. J. Meath, J. C. F. McDonald, and D. J. Dawson, Can. J. Phys. **55**, 2080 (1977).

[63] A. Kumar, B. L. Jhanwar, and W. J. Meath, Can. J. Chem. **85**, 724 (2007).

[64] D. J. Margoliash and W. J. Meath, J. Chem. Phys. **68**, 1426 (1978).

[65] A. Kumar and W. J. Meath, Mol. Phys. **54**, 823 (1985).

[66] A. Kumar, J. Mol. Struct.: THEOCHEM **591**, 91 (2002).

[67] G. D. Zeiss and W. J. Meath, Mol. Phys. **33**, 1155 (1977).

[68] A. Kumar, M. Kumar, and W. J. Meath, Mol. Phys. **101**, 1535 (2003).

[69] A. Kumar, M. Kumar, and W. J. Meath, Chem. Phys. **286**, 227 (2003).

[70] A. Kumar, G. R. G. Fairkey, and W. J. Meath, J. Chem. Phys. **83**, 70 (1985).

[71] B. L. Jhanwar and W. J. Meath, Mol. Phys. **41**, 1061 (1980).

[72] A. Kumar and W. J. Meath, Mol. Phys. **75**, 311 (1992).

[73] V. Blum, R. Gehrke, F. Hanke, P. Havu, V. Havu, X. Ren, K. Reuter, and M. Scheffler, Comput. Phys. Commun. **180**, 2175 (2009).

[74] W. Humphrey, A. Dalke, and K. Schulten, J. Mol. Graphics **14**, 33 (1996); VMD version 1.8.6., http://www.ks.uiuc.edu/research/vmd/.

[75] See: http://sourceforge.net/ for GDIS code.

[76] L. A. Schwalbe, R. K. Crawford, H. H. Chen, and R. A. Aziz, J. Chem. Phys. **66**, 4493 (1977).

[77] O. G. Peterson, D. N. Batchelder, and R. O. Simmons, Phys. Rev. **150**, 703 (1966).

[78] E. G. Cox, Rev. Mod. Phys. **30**, 159 (1958).

[79] M. T. Yin and M. L. Cohen, Phys. Rev. B **24**, 6121 (1981).

[80] K. Thürmer and N. C. Bartelt, Phys. Rev. B **77**, 195425 (2008).

[81] P. J. Feibelman, Phys. Chem. Chem. Phys. **10**, 4688 (2008).

[82] R. Zacharia, H. Ulbricht, and T. Hertel, Phys. Rev. B **69**, 155406 (2004).

[83] W. Branz, N. Malinowski, A. Enders, and T. P. Martin, Phys. Rev. B **66**, 094107 (2002).

[84] I.-C. Lin, O. A. von Lilienfeld, M. D. Coutinho-Neto, I. Tavernelli, and U. Rothlisberger, J. Phys. Chem. B **111**, 14346 (2007).

[85] R. Podeszwa and K. Szalewicz, J. Chem. Phys. **126**, 194101 (2007).

[86] D. D. Richardson, J. Phys. C **11**, 3779 (1978).

[87] B. Santra, A. Michaelides, M. Fuchs, A. Tkatchenko, C. Filippi, and M. Scheffler, J. Chem. Phys. **129**, 194111 (2008).

[88] J. Ireta, J. Neugebauer, M. Scheffler, A. Rojo, and M. Galvan, J. Am. Chem. Soc. **127**, 17241 (2005).

[89] P. Cieplak, F. Dupradeau, Y. Duan, and J. Wang, J. Phys.: Condens. Matter **21**, 333102 (2009).

[90] A. Grosdidier, V. Zoete, and O. Michielin, J. Comput. Chem. **30**, 2021 (2009).

[91] V. Zoete, A. Grosdidier, and O. Michielin, J. Cell. Mol. Med. **13**, 238 (2009).

[92] O. A. von Lilienfeld, R. Lins, and U. Rothlisberger, Phys. Rev. Lett. **95**, 153002 (2005).

[93] O. A. von Lilienfeld and M. E. Tuckerman, J. Chem. Phys. **125**, 154104 (2006).

[94] O. A. von Lilienfeld and M. E. Tuckerman, J. Chem. Theory Comput. **3**, 1083 (2007).

[95] S. L. Price, Adv. Drug Delivery Rev. **56**, 301 (2004).

[96] M. A. Neumann, F. J. J. Leusen, and J. Kendrick, Angew. Chem., Int. Ed. **47**, 2427 (2008).

[97] M. A. Neumann and M.-A. Perrin, J. Phys. Chem. B **109**, 15531 (2005).

[98] Y. Wang and J. P. Perdew, Phys. Rev. B **44**, 13298 (1991).

[99] J. P. Perdew, J. A. Chevary, S. H. Vosko, K. A. Jackson, M. R. Pederson, D. J. Singh, and C. Fiolhais, Phys. Rev. B **46**, 6671 (1992).

[100] W. M. Brown, A. P. Thompson, and P. A. Schultz, J. Chem. Phys. **132**, 024108 (2010).

[101] O. Borodin, G. D. Smith, T. D. Swell, and D. Bedrov, J. Phys. Chem. B **112**, 734 (2008).

[102] S. W. Rick and S. J. Stuart, Rev. Comput. Chem. **18**, 89 (2002).

[103] V. N. Staroverov, G. E. Scuseria, J. Tao, and J. P. Perdew, Phys. Rev. B **69**, 075102 (2004).

[104] S. Kristyán and P. Pulay, Chem. Phys. Lett. **229**, 175 (1994).

[105] J. M. Pérez-Jordá and A. D. Becke, Chem. Phys. Lett. **233**, 134 (1995).

[106] Y. Zhao and D. G. Truhlar, J. Chem. Theory Comput. **1**, 415 (2005).

[107] J. Hepburn, G. Scoles, and R. Penco, Chem. Phys. Lett. **36**, 451 (1975).

[108] R. LeSar, J. Phys. Chem. **88**, 4272 (1984).

[109] M. Elstner, D. Porezag, G. Jungnickel, J. Elsner, M. Haugk, T. Frauenheim, S. Suhai, and G. Seifert, Phys. Rev. B **58**, 7260 (1998).

[110] D. Sánchez-Portal, P. Ordejón, E. Artacho, and J. M. Soler, Int. J. Quantum Chem. **65**, 453 (1997).

[111] M. Elstner, P. Hobza, T. Frauenheim, S. Suhai, and E. Kaxiras, J. Chem. Phys. **114**, 5149 (2001).

[112] X. Wu, M. C. Vargas, S. Nayak, V. Lotrich, and G. Scoles, J. Chem. Phys. **115**, 8748 (2001).

[113] M. Hasegawa and K. Nishidate, Phys. Rev. B **70**, 205431 (2004).

[114] S. Grimme, J. Comput. Chem. **25**, 1463 (2004).